Journal of Medicinal Chemistry

Brief Article

An Unusual Binding Model of the Methyl 9-Anilinothiazolo[5,4-f] quinazoline-2-carbimidates (EHT 1610 and EHT 5372) Confers High Selectivity for Dual-specificity Tyrosine Phosphorylation-Regulated Kinases.

Apirat Chaikuad, Julien Diharce, Martin Schröder, Alicia Foucourt, Bertrand Leblond, Anne-Sophie Casagrande, Laurent Desire, Pascal Bonnet, Stefan Knapp, and Thierry Besson

J. Med. Chem., **Just Accepted Manuscript** • DOI: 10.1021/acs.jmedchem.6b01083 • Publication Date (Web): 21 Oct 2016

ACS Publications

Journal of Medicinal Chemistry is published by the American Chemical Society. 1155 Sixteenth Street N.W., Washington, DC 20036

An Unusual Binding Model of the Methyl 9-Anilinothiazolo[5,4-*f*] quinazoline-2-carbimidates (EHT 1610 and EHT 5372) Confers High Selectivity for Dual-specificity Tyrosine Phosphorylation-Regulated Kinases.

Apirat Chaikuad,[†] Julien Diharce,[‡] Martin Schröder, [¥] Alicia Foucourt,[§] Bertrand Leblond,[ǀ] Anne-Sophie Casagrande,[ǀ] Laurent Désiré,[ǀ] Pascal Bonnet,[‡] Stefan Knapp,*[,†,¥] Thierry Besson*[,§]

[†] Target Discovery Institute (TDI), and Structural Genomics Consortium (SGC), University of Oxford, Old Road Campus Research Building, Oxford OX3 7DQ, U.K.
[‡] Institut de Chimie Organique et Analytique, UMR CNRS-Université d'Orléans 7311, Université d'Orléans BP 6759, Orléans 45067 Cedex 2, France
[¥] Institute of Pharmaceutical Chemistry and Buchman institute for life sciences, Goethe-University, Max-von-Laue-Str. 9, 60438 Frankfurt am Main, Germany
[§] Normandie Univ, UNIROUEN, INSA Rouen, CNRS, COBRA UMR 6014, 76000 Rouen, France
[ǀ] Diaxonhit, 63-65 Boulevard Masséna, 75013 Paris, France

KEYWORDS: DYRK1A, DYRK1B, DYRK2, thiazolo[5,4-*f*]quinazoline

ABSTRACT: Methyl 9-anilinothiazolo[5,4-*f*]quinazoline-2-carbimidates **1** (EHT 5372) and **2** (EHT 1610) are strong inhibitors of DYRK's family kinases. The crystal structures of the complex revealed a non-canonical binding mode of compound **1** and **2** in DYRK2 explaining the remarkable selectivity and potency of these inhibitors. The structural data and comparison presented here provide therefore a template for further improvement of this inhibitor class and for the development of novel inhibitors selectively targeting DYRK kinases.

Protein kinases catalyze protein phosphorylation, a key cellular regulatory mechanism, which is frequently dysregulated in human diseases. Kinases have therefore been linked to the development of a variety of diseases including cancer, neurodegenerative disorders and cardiovascular diseases.[1-3] Consequently, protein kinases represent pertinent targets for academic and industrial chemists developing inhibitors as potential new therapeutic agents.[4,5] Most kinases target serine (Ser) and threonine (Thr) residues as substrates, others specifically phosphorylate tyrosines (Tyr) and a number (dual-specificity kinases or DYRKs) may phosphorylate under certain circumstances all three residues. DYRKs belong to the CMGC group of Ser/Thr kinases, which also includes cyclin-dependent kinases (CDKs), mitogen-activated protein kinases (MAPKs), glycogen synthase kinases (GSKs) and CDC2-like kinases (CLKs). During translation and folding, DYRKs auto-phosphorylate their own activation loop on a tyrosine residue. After this initial tyrosine phosphorylation DYRKs convert to Ser/Thr kinases.[6,7] In human, the DYRK family includes five members: DYRK1A, DYRK1B, DYRK2, DYRK3 and DYRK4 and the more distantly member Pre-MRNA Processing Factor 4 (PRP4). All share considerable sequence identity in their kinase domain.[8] DYRK1A is certainly the most studied family member and has attracted considerable interest due to its role in Down syndrome pathology and its suspected role in neurodegenerative diseases, cancer[9] and diabete.[10]

DYRK1A has been shown to phosphorylate more than thirty proteins to regulate diverse biological functions, including synaptic transmission, neurodegeneration, transcription, mRNA splicing, cell proliferation and survival.[11-13] DYRK1B (also called Mirk for Minibrain-related kinase) is potentially an attractive cancer target that is highly expressed in quiescent cancer cells while it is expressed at very low levels in normal tissue. It has been hypothesized that pharmacological DYRK1B inhibition would enable cancer cells to escape from quiescence, triggering apoptosis, and re-sensitize cancer cells to conventional chemotherapeutic agents.[14]

An important role of DYRK1A in a number of diseases and the unknown functions of other family members have prompted an interest in the development of potent and selective inhibitors for DYRK kinases. Since the discovery of a plant alkaloid harmine as potent DYRK1A inhibitor with IC_{50}s of 30-80 nM,[15,16] a number of efforts have led to diverse potent inhibitors, including INDY,[17] natural product leucettine L41,[18] pyrido[2,3-*d*]pyrimidines-based inhibitors[19] with reported IC_{50}s in the range of 9-240 nM. However, these early inhibitors often significantly cross-react with other kinases such as GSK3β and CLKs and in the case of harmine with other enzymes. Recently, the discovery of a new chemical class has led to another potent and selective DYRK1A inhibitor, 10-iodo-11*H*-indolo[3,2-c]quinoline-6-carboxylic acid (known also as inhibitor 5j), with a reported IC_{50} of 6 nM demonstrating at least 80-fold more potency over other related kinases.[20] Nonetheless, an obstacle for its use is its poor cellular activity.

Our previous efforts have demonstrated the usefulness of thiazolo[5,4-*f*]quinazolines for the development of GSK3β and CDK1 inhibitors.[21,22] We further considered a possible use of this chemical scaffold towards the development of DYRKs inhibitor since these kinases share some similarity and belong to the same CMGC family. DYRK1A and 1B were our targets of

interest due to their strong links to diseases. However, their high sequence identity of ~85% suggested that isoform selective inhibitors could represent a big challenge; hence we limited our aim in this current study to dual inhibitors, allowing to focus on the synthetic chemistry. To functionalize and decorate the scaffold, we applied our previously described microwave-assisted synthetic routes and the use of Appel salt (4,5-dichloro-1,2,3-dithiazolium chloride) for the conception of a 6-amino-2-cyanobenzo[*d*]thiazole-7-carbonitrile derivative as a versatile molecular platform from 5-nitroanthranilonitrile. The introduction of various aliphatic, aromatic or amino substituents at position 8 was best achieved by a one-pot DMFDMA-mediated cyclisation.[23] Transformation of carbonitrile group into various chemical functions (*e.g.* imidate, ester, amide and amidine) allowed the efficient preparation of a library of 110 novel methyl 9-anilinothiazolo[5,4-*f*]quinazoline-2-carbimidate derivatives.[24-26]

We previously tested this library for their effectiveness against DYRK1A and DYRK1B, and most of them showed similar or better inhibitory potency compared to harmine.[25,26] Interestingly, among them the five most active molecules prepared in this study were **1** (EHT 5372), **2** (EHT 1610), **3** (EHT 9851), **4** (EHT 6840) and **5** (EHT 3356) which harbored a phenyl group at ^{9}N which was disubstituted in *ortho* and *para* by halogen atoms (Cl and F) (Figure 1). In the case of **2** (EHT 1610) a fluor atom in *ortho* was accompanied by a methoxy group in *para* and in the case of **5** (EHT 3356) only a methyl group in the *para* position.[24-26] These compounds exhibited strong potency with IC_{50} values in the sub-nanomolar to single-digit nanomolar range for DYRK1A (0.22-0.99 nM) and DYRK1B (0.28-2.83 nM).

Among the five top hits, the most potent inhibitors in this series were methyl 9-(2,4-dichlorophenylamino)thiazolo[5,4-*f*]quinazoline-2-carbimidate (**1**) and methyl 9-(2-chloro,4-methoxyphenylamino)thiazolo[5,4-*f*]quinazoline-2-carbimidate (**2**) that exhibited IC_{50}s of 0.22/0.28 nM and 0.36/0.59 nM for DYRK1A/1B, respectively.

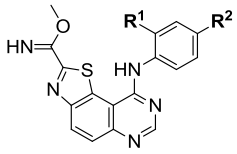

Compound	R^1	R^2	DYRK1A / 1B*
1 (EHT 5372)	Cl	Cl	0.22 / 0.28
2 (EHT 1610)	F	OMe	0.36 / 0.59
3 (EHT 9851)	F	F	0.94 / 1.07
4 (EHT 6840)	F	Cl	0.99 / 1.63
5 (EHT 3556)	H	Me	0.98 / 2.83
Harmine			21.83 / 57.4
Leucettine L41			7.60 / 37.0

* IC_{50} (nM)

Figure 1. Chemical structures of methyl 9-anilinothiazolo[5,4-*f*]quinazoline-2-carbimidates **1**-**5** and DYRK1A and DYRK1B IC_{50} (nM) values.

We next examined their potency and selectivity against a small panel of closely-related kinases, including for example DYRK1A, DYRK2, PRP4, CLK1/3, GSK3α/β, PIM1, SRPK1, using differential scanning fluorimetry (DSF) (Tm shift assay). As expected, both compounds showed good binding to their target DYRK1A with Tm shift of ~9 °C and demonstrated a good selectivity (Figure 2A). However, we also observed interaction of three off-targets, DYRK2, CLK1 and GSK3β, albeit with significantly smaller Tm shifts in the range of 5-6 °C. The observed good selectivity to closely related kinases was in agreement with our comprehensive kinome wide screening study, which showed remarkably high selectivity over 339 kinases.[27] Interestingly, both independent assays detected a similar set of off-targets with significantly weaker inhibition (IC_{50}s in the range of 3.2- >1,570 nM) which was supported by the lower Tm shift observed here (Figure 2B).

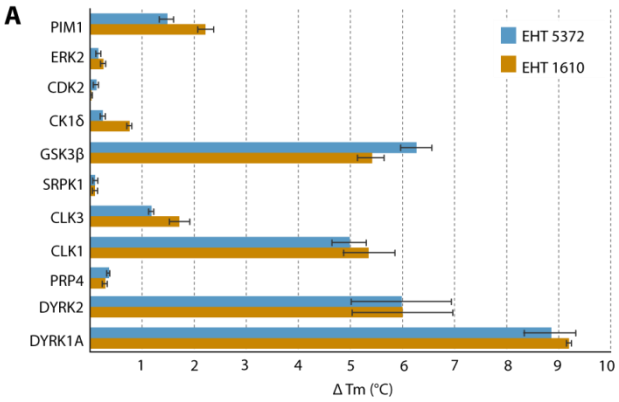

B

IC50 (nM)	DYRK1A	DYRK1B	DYRK2	DYRK3	DYRK4	CLK1	CLK2	CLK3	CLK4	GSK3α	GSK3β
EHT 5372 [a]	0.22	0.28	10.8	93.2	n/a	22.8	88.8	>10000	59.0	7.44	221
EHT 1610	0.36	0.59	3.16	21.1	1570	11.0	32.5	1420	32.0	9.11	143

Figure 2 Selectivity analysis of compound **1** and **2**: Tm shifts (**A**) and IC_{50} values (**B**) for selected kinases screened against compounds **1** and **2**. n/a = no inhibition detected, [a] values from Ref. 27.

Furthermore, we also observed remarkable selectivity within DYRKs family. DYRK2 was the strongest off-target with IC_{50}s for **1** and **2** of 10.8 and 3.16 nM, respectively, which was despite the high homology still ~38- and 5-fold weaker when compared to DYRK1A/1B. Of particular interest were differences in selectivity and potency of **1** and **2**. One of the main differences between these compounds was a substitution of the Cl and methoxy groups at the R^2 position, respectively. Switching halide to methoxy groups led to lower inhibitory effect for DYRK1A/1B by ~2-fold. On the contrary, this substitution instead significantly increased the potency towards other off-targets, essentially DYRK2.

To provide the structural insights into the binding modes of these two inhibitors, we attempted to co-crystallize **1** and **2** with DYRK1A, but did not succeed to obtain crystals that diffracted to high resolution. We therefore performed co-crystallization of both compounds with DYRK2, and this led to successful structure determination of the DYRK2-**1** and -**2** complexes to 2.15 and 2.58 Å resolution, respectively (Supplementary Table S1).

We observed interpretable electron density for both ligands (Figure 3A), allowing confident modelling of the inhibitors within the pocket. The binding modes of both inhibitors were remarkably similar (Figure 3B).

In brief, the heterocyclic thiazolo[5,4-*f*]quinazoline was located deep within the ATP binding site, and sandwiched by Val163 and Ile294. This orientation placed the thiazolo adjacent to the gatekeeper Phe228, and positioned the N1 nitrogen group of the quinazoline ring for a hydrogen bond interaction within the salt bridge Lys178. The methyl-carbimidate decoration pointed towards the hinge with its nitrogen group at 3.1-3.6 Å

away from the backbone of the hinge residues Glu229 and Leu231, thus not interacting strongly with the hinge region.

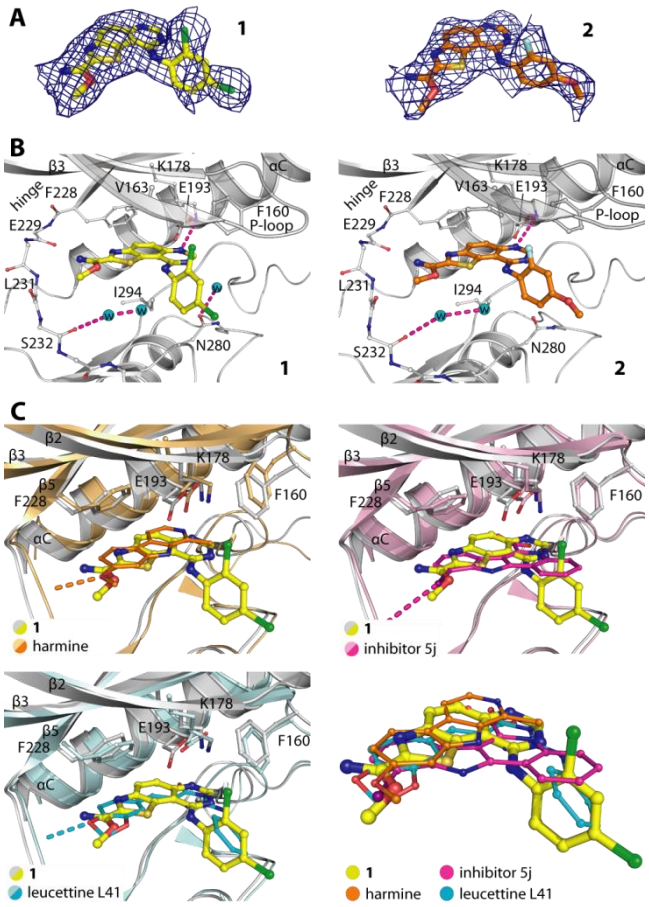

Figure 3 Crystal structures of DYRK2 in complexes with **1** and **2. A)** $|F_O|$-$|F_C|$ omitted map contoured at 3.0σ for the bound inhibitors. **B)** Detailed interactions of the binding modes of the inhibitors with DRYK2. Magenta, dashed lines indicates potential hydrogen bonds, and water molecules are shown as cyan spheres. **C)** Superimposition of DYRK2-**1**, DYRK1A-harmine (pdb id: 3ANR), DYRK1A-inhibitor 5j (pdb id: 4YLJ) and DYRK1A-leucettine L41 (pdb id: 4AZE) reveals that **1** occupies large space inside the DYRK ATP pocket. Note that numbering is according to DYRK2.

In contrast, optimal hydrogen interactions were observed in the backpocket where the quinazoline nitrogen was engaged in a hydrogen bond network with conserved lysine/glutamate ion pair. In addition, the aromatic gatekeeper (Phe228) formed a π-π-stacking interaction with the central aromatic ring system of the inhibitor. The 2-chloro or 2-fluoro R^1 decoration of this group was ~3.3-3.7 Å away from the P-loop Phe160 that was observed to adopt a distorted 'folded-in' conformation, a structural alteration which has been reported to often confer selectivity. Conversely, the chloro or methoxy decoration at R^2 position pointed outwards to the solvent exterior with no interaction observed.

The observed binding mode provided no direct evidence on why this R^2 substitution altered potency and selectivity between these two inhibitors. However, the observed ~21-30° tilt of the aniline group suggested that the change of charges, size and van der Waal radii in this position most likely affects interaction within the cavity created between the P-loop and the C-lobe αD and β7, which often possess significantly different features among different kinases. In addition, the difference in size and electrostatic property of the halides at R^1 position could also contribute their effects towards the affinities when bound in proximity to the aromatic Phe160.

The observed binding mode of the core thiazolo[5,4-*f*]quinazoline scaffold in DYRK2 was rather unexpected when compared to the predicted binding mode of a similar derivative in GSK3β, where the heterocyclic core was proposed to adopt a canonical hinge binding with the quinazoline interacting with the hinge backbone pointing the carbimidate towards the catalytic salt bridge for potential hydrogen bond.[21,22] The flip of the ring in DYRK2 resulted in a loss of strong canonical hinge interaction, yet maintain a hydrogen bond to the salt bridge but through the quinazoline moiety. Such different accommodation mechanisms of the core ATP-mimetic scaffold between these two kinases could form a basis of selectivity between DYRKs and other closely-related kinases. However, it should be noted that the binding mode of this core scaffold in GSK3β was based on a docking study, unlike that in DYRK2, which was observed in the crystal structures. We then compared the binding modes of these compounds with other known DYRK inhibitors, including harmine, leucettine L41 and inhibitor **5j**. Structural comparison revealed that all inhibitors did superimpose well with similarity regarding the planarity and orientation of their core scaffolds (Figure 3C). In essence, the binding geometry of our compounds highly resembled that of leucettine L41, of which the phenyl group adopted also a nearly-perpendicular vertical conformation in a similar manner to the aniline moiety of our inhibitors. Interestingly, unlike **1** and **2**, other known inhibitors maintain a hinge interaction either via hydrogen or halogen bond.

To provide the binding modes of **1** and **2** in the target DYRK1A/1B, we performed docking studies with DYRK1A, and that coupled with structural modelling of DYRK1B (see Supporting Information). The calculated models revealed that both inhibitors assumed identical binding modes as those observed in the crystal structures of DYRK2 (Figure 4).

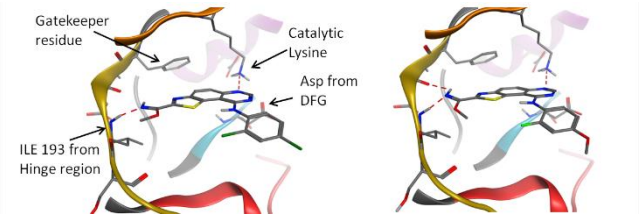

Figure 4. Modelling of **1** and **2** with DYRK1A/1B. Potential binding modes of **1** (left) and **2** (right) in DYRK1B calculated from structural modelling and docking studies (Yellow: Hinge region, Red: Catalytic loop, Blue: DFG motif, Purple: α-C Helix, Orange: Catalytic lysine).

The core thiazolo[5,4-*f*]quinazoline would adopt the similar planar geometry, with the quinazoline engaging a hydrogen bond with the salt bridge lysine. Interestingly, we predicted that the carbimidate nitrogen forms improved canonical hinge interaction with the hinge backbone of Ile241 or Ile193 in DRYK1A and 1B. This observation could be the structural basis of the significant increase in affinities of both inhibitors towards DYRK1A/1B. Based on our docking data, the aniline moiety

assumed several conformations due to its position in proximity to solvent-exposed area, again offering no direct evidence why the R^2 chloro- and methoxy-substitution altered affinities by ~2-3 fold.

Overall structural comparison suggested that the canonical hinge may be less essential for high affinity binding in DYRKs. The unusual binding mechanisms of **1** and **2** occupied a large portion of the ATP binding pocket, essentially covering nearly all cavities targeted by the other three inhibitors compared here (Figure 3C). Calculations of the changes of solvent-accessible surface area (SASA) due to ligand binding revealed that compounds **1** and **2** are 92% and 88% buried in DYRK2, and by docking 86% and 83% binding to DYRK1A, respectively.

In addition, studies of the thermodynamics of the unusual binding mode by isothermal titration calorimetry (ITC) revealed also that inhibitor binding was driven by a large negative binding enthalpy. The Kd was determined to be 7.4 ±4 nM. However, due to the high affinity of **2** the affinity measurements were associated with a large error. The indirectly determined entropy term (TΔS) was unfavorable. (Figure 5).

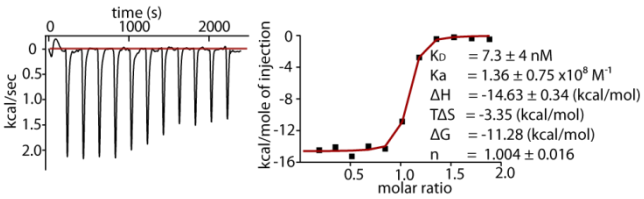

Figure 5. ITC binding data of 2 with DYRK1A. Shown are the isotherms of raw titration heat (left), and the normalized binding heat with the single-site fitting (red line) (right).

We next performed the sequence alignment of the kinase domains of DYRK1A, DYRK1B, DYRK2, DYRK3 and DYRK4 to analyze the basis of selectivity of the inhibitors within DYRK family. The results revealed a well-conserved active site of the DYRK1 and DYRK2 subfamilies (Figure 6A). Further analyses revealed that DYRK1A and DYRK1B had a higher percentage of identity and similarity of 85.0% and 93.1%, respectively, and this was the case also for DYRK2 and DYRK3 (identity = 79.0%, similarity = 89.5%). DYRK4 was an outlier in the family, sharing <60% and <80% sequence identity and similarity, respectively, to other members (Figure 6B). Based on this statistics, it was therefore possible to classify the kinases into 3 clusters; i) DYRK1A/1B, ii) DYRK2/3 and iii) DYRK4. This result from sequence alignment was consistent with the trend in affinities of both inhibitors with no or weak inhibition for DYRK4, moderate binding for DYRK2/3 and high potency for DYRK1A/1B. Since no crystal structure is currently available for this kinase, we postulated that overall features and environment of the ATP pocket of DYRK4 is significantly different from that of the other DYRKs. Despite low sequence identity and similarity, the possible binding with moderate potency of the inhibitors in DYRK2 was supported by the similarity in environment of the ATP pocket to that of DYRK1A. However, subtle differences at the backpocket between DYRK2/3 and DYRK1A/1B clusters, including the residue before DFG motif (DYRK2 Ile294/ DYRK1A Val306) and the residue at the beginning of β4 (DYRK2 Ile212/ DYRK1A Val222), might form the basis of a significant change in affinities between these two subclasses.

Since the inhibitors interacted with these residues in the back-pocket, the bulkier sizes of isoleucine in DYRK2 could lead to more steric hindrance compared to the smaller valine in DYRK1A. Indeed, *in silico* mutation demonstrated that the substitution of the corresponding DYRK1A/B valine into isoleucine caused a subtle shift of the binding positions of the inhibitors in comparison to that of the wildtype. This observation support differences in the observed inhibitor potencies between the DYRK1A/1B and DYRK2/3. Nonetheless, further experiments may be required to fully understand the impact of these differences on the binding mode of **1** and **2** within these two DYRKs sub-families.

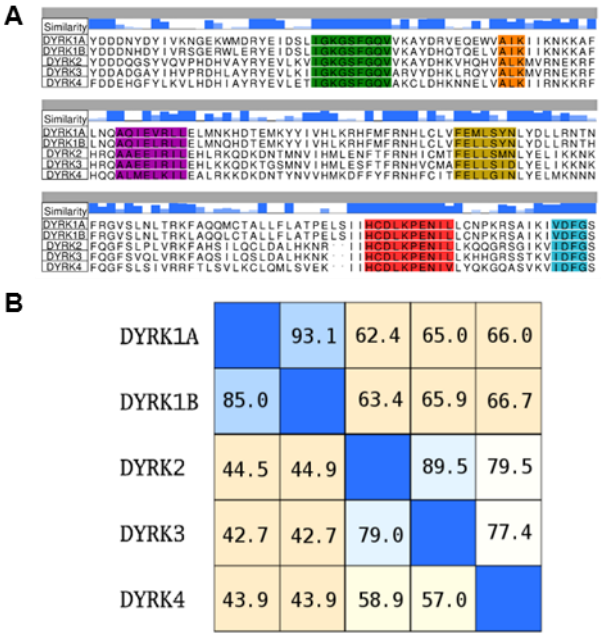

Figure 6. Sequence alignment of DYRK family. **A)** Sequence alignment of the region within the ATP binding pockets of DYRK family. Sequence similarity (%) to other DYRK kinases is represented by a blue bar. **B)** Percentages of identity (bottom left quadrant) and similarity (top right quadrant) of kinase domain sequences from members of DYRK1 and DYRK2 subfamilies.

To our knowledge, the two compounds presented here are the most potent and selective DYRK1A/1B inhibitors reported to date. We have previously demonstrated that **1** was active in cells, and inhibited DYRK1A-induced Tau phosphorylation at multiple sites in biochemical assay, cell lines, and primary cortical neurons without affecting cell viability. Inhibitor **1** compared favorably to harmine, leucettine L41 and to the reactive and promiscuous compound epigallo-catechin-gallate EGCG[27] In addition, it normalized Aβ-induced Tau phosphorylation in neuronal cells and also normalized DYRK1A-induced Aβ production in APP over-expressing cells.[27] In addition, *in vitro* characterization in various cancer cellular models showed that the inhibitor targeted G0/G1 transition and reduced stemness and EMT properties of cancer cells organized in spheroids.[28] Furthermore, it demonstrated promising activities in patient-derived ovarian cancer ascites spheroids and *in vivo* activities in a Panc1 xenograft model without detectable toxicity in mice.[29] Similar to **1**, the compound **2** has been previously observed to dose-dependently inhibit DYRK1A in both B- and T-lineage

acute lymphoblastic leukemia (ALL).[30] In addition, the inhibitors also induced apoptosis of primary ALL cells that were resistant to cytarabine, suggesting that DYRK1A inhibitors may be used in combination with standard ALL therapies for refractory or relapsed cases.[29] These results suggested that both compounds not only exhibited high potency *in vitro*, but demonstrated also good activities in cell based systems and *in vivo* models. These data therefore suggest a potential use of this class of inhibitors for targeting cancer cells with high DYRK1A/1B kinase activities.[27-33]

EXPERIMENTAL SECTION

Complete and detailed synthesis of inhibitors **1** (EHT 5372) and **2** (EHT 1610) used in this study have been described in ref. 24, 25 and 26. The target compounds **1** and **2** were obtained in nine steps from 5-nitroanthranilonitrile in overall yields of 6 % and 14 %, respectively.

General procedures. Materials were obtained commercially and used without further purification. All reactions were carried out under inert atmosphere of argon or nitrogen and monitored by thin-layer chromatography with silica gel 60 F254 pre-coated aluminium plates (0.25 mm). Visualization was performed with a UV light at 254 and 312 nm. Purifications were carried out by flash column chromatography system equipped with a dual UV-Vis spectrophotometer (200-600 nm), a frion collector (176 tubes), a dual pistopump (1 to 200 mL/min, Pmax = 15 bar) allowing quaternary gradients and an additional inlet for air purge. Samples can be injected in liquid or solid mode. Melting points of solid compounds were measured on a STUART Melting Point SMP3 with a precision of +/- 1.5 °C. IR spectra were recorded on a PerkinElmer Spectrum 100 Series FT-IR spectrometer. Liquids and solids were applied on the Siction Attenuated Total Reflectance (ATR) Accessories. Absorption bands are given in cm^{-1}. ^{1}H, ^{19}F NMR spectra were recorded at 295 °K on a Bruker AVANCE 300 MHz, at 300 relative to $CDCl_3$ (residual solvent signals). Mass spectra analysis was performed by the Mass Spectrometry Laboratory of the University of Rouen. Mass spectra (ESI) were recorded with a Waters LCP 1er XR spectrometer. Microwave experiments were conducted at atmospheric pressure (RotoSYNTH™, Milestone S.r.l. Italy) or in pressurized reactors (0-30 bars) (Monomode 300™, Anton Paar, France) in commercial microwave reactors especially designed for synthetic chemistry. The purity of all tested compound was determined by chromatographic analysis performed at 25 °C on Ultimate 3000 (Thermo Scientific, Les Ulis, France) with a binary pump, photodiode array detector (DAD) managed at 289 nm. Column was a Pursuit XRS (250 mm × 4.6 mm; 5 µm particle size) provided by Varian (Les Ulis, France). The mobile phase was H_2O/AcCN (40:60; v/v). Flow rate was 1 mL/min and 20 µL were injected. The percentage of purity of all products was more than 96%.

Methyl 9-(2,4-dichlorophenylamino)thiazolo[5,4-f]quinazoline-2-carbimidate (**1**). Flash chromatography eluent (EtOAc). Yellow solid. Overall yield: 6%, mp > 260 °C. IR (cm^{-1}) ν_{max} 2953, 1727, 1641, 1586, 1507, 1488, 1464, 1394, 1354, 1284, 1158, 1099, 1073, 1054, 941, 860, 816; ^{1}H-NMR (300 MHz, DMSO-d_6) δ 9.34 (s, 1H, NH), 8.45 (d, 1H, *J* = 9.0 Hz), 8.10 (s, 1H), 7.72 (d, 1H, *J* = 9.0 Hz), 7.61 (s, 1H), 7.37 (d, 1H, *J* = 8.1 Hz), 7.18 (d, 1H, *J* = 8.1 Hz), 3.94 (s, 3H); HRMS calcd for $C_{17}H_{12}N_5OSCl_2$ $[M + H]^+$: 404.0140, found 404.0146.

Methyl 9-(2-fluoro-4-methoxyphenylamino)thiazolo[5,4-f]quinazoline-2-carbimidate (**2**). Flash chromatography eluent (EtOAc). Yellow solid. Overall yield: 14%, mp = 224-226°C (isopropanol). IR (cm^{-1}) ν_{max} 3150, 2950, 1645, 1601, 1570, 1488, 1435, 1355, 1322, 1285, 1269, 1203, 1155, 1096, 1069, 1032, 939, 819; ^{19}F NMR (282 MHz, DMSO-d_6) δ -120.44; ^{1}H NMR (300 MHz, DMSO-d_6) δ 9.22 (s, 1H, NH), 8.28 (d, 1H, *J* = 9.0 Hz), 8.06 (s, 1H), 7.62 (d, 1H, *J* = 9.0 Hz), 7.39 (m, 1H), 6.81 (dd, *J* = 9.0, 3.0 Hz, 1H), 6.71 (dd, *J* = 9.0, 3.0 Hz, 1H), 3.94 (s, 3H), 3.75 (s, 3H); HRMS calcd for $C_{18}H_{15}N_5O_2SF$ $[M + H]^+$: 384.0927, found 384.0930.

ASSOCIATED CONTENT

The Supporting Information is available free of charge on the ACS Publications website at DOI:

Detailed synthesis of compounds **1** (EHT 5372) and **2** (EHT 1610), ^{1}H NMR spectra and HPLC chromatograms for compounds **1** and **2**, details of docking experiments, protein expression and purification, thermal stability assays, docking experiments of **1** and **2** in DYRK1A and DYRK1B, isothermal titration calorimetry.

The structure coordinates have been deposited in the protein Data Bank accession code: 5LXC and 5LXD

AUTHOR INFORMATION

Corresponding Authors

*Phone: +33 (0)235 622 904. E-mail: thierry.besson@univ-rouen.fr

*Phone: +49 69798-29871. E-mail: knapp@pharmchem.uni-frankfurt.de

Mail Address

† Laboratoire COBRA, UMR CNRS 6014, Université de Rouen, Bâtiment IRCOF, 1 rue Tesnière, F-76821 Mont Saint-Aignan Cedex, FRANCE.

Author Contributions

T.B. and B.L. conceived and designed the project. All authors have given approval to the final version of the manuscript.

Funding Sources

A.F. P.B. and T.B. are supported by LABEX SynOrg (ANR-11-LABX-0029).

Financial support from the MESR (*Ministère de l'Enseignement Supérieur & de la Recherche*) is gratefully acknowledged for the doctoral fellowships to A.F. AC is supported by the EU network fellowship PRIMES. SK is grateful for supported by the SGC, a registered charity (number 1097737) that receives funds from AbbVie, Bayer Pharma AG, Boehringer Ingelheim, Canada Foundation for Innovation, Eshelman Institute for Innovation, Genome Canada through Ontario Genomics Institute, Innovative Medicines Initiative (EU/EFPIA) [ULTRA-DD grant no. 115766], Janssen, Merck & Co., Novartis Pharma AG, Ontario Ministry of Economic Development and Innovation, Pfizer, São Paulo Research Foundation-FAPESP, Takeda, and the Wellcome Trust as well as the Innovative Medicines Initiative (EU/EFPIA) grant K4DD.

Notes

The authors declare no competing financial interest.

ACKNOWLEDGMENTS

Financial support from the MESR (*Ministère de l'Enseignement Supérieur & de la Recherche*) is gratefully acknowledged for the doctoral fellowships to A.F. AC is supported by the EU network fellowship PRIMES. SK is grateful for supported by the SGC, a registered charity (number 1097737) that receives funds from AbbVie, Bayer Pharma AG, Boehringer Ingelheim, Canada Foundation for Innovation, Eshelman Institute for Innovation, Genome Canada through Ontario Genomics Institute, Innovative Medicines Initiative (EU/EFPIA) [ULTRA-DD grant no. 115766], Janssen,

Merck & Co., Novartis Pharma AG, Ontario Ministry of Economic Development and Innovation, Pfizer, São Paulo Research Foundation-FAPESP, Takeda, and the Wellcome Trust as well as the Innovative Medicines Initiative (EU/EFPIA) grant K4DD. We thank the staffs at Diamond Light Source, Beamline I04-1 for assistance during data collection.

ABBREVIATIONS USED

DMFDMA, dimethylformamidedimethylacetamide; DYRKs, dual specificity tyrosine phosphorylation-regulated kinases; EMT, epithelial-Mesenchymal transition. CLK, cdc2 like kinases.

REFERENCES

(1) Martin, L.; Latypova, X.; Wilson, C.M.; Magnaudeix, A.; Perrin, M.-L.; Terro, F. Tau protein kinases: Involvement in Alzheimer's disease. *Ageing Res. Rev.* **2013**, *12*, 289–309.

(2) Flajolet, M.; He, G.; Heiman, M.; Lin, A.; Nairn, A.C.; Greengard, P. Regulation of Alzheimer's disease amyloid-β formation by casein kinase I. *Proc. Nat. Acad. Sci. USA* **2007**, *104*, 4159–4164.

(3) Weinmann, H.; Metternich, R. Drug discovery process for kinase Inhibitors. *ChemBioChem* **2005**, *6*, 455–459.

(4) Wu, P.; Nielsen, T.E.; Clausen, M.H. Small-molecule kinase inhibitors: an analysis of FDA-approved drugs. *Drug Discov. Today* **2016**, *21*, 5–10.

(5) Wu, P.; Nielsen, T.E.; Clausen, M.H. FDA-approved small-molecule kinase inhibitors. *Trends Pharmacol. Sci.* **2015**, *36*, 422–439.

(6) Rüben, K.; Wurzlbauer, A.; Walte, A.; Sippl, W.; Bracher, F.; Becker, W. Selectivity profiling and biological activity of novel β-carbolines as potent and selective DYRK1 kinase inhibitors. *PLoS ONE* **2015**, *10*, e0132453; DOI: 10.1371/journal.pone.0132453.

(7) Varjosalo, M.; Keskitalo, S.; Van Drogen, A.; Nurkkala, H.; Vichalkovski, A.; Aebersold, R.; Gstaiger, M. The protein interaction landscape of the human CMGC kinase group. *Cell Rep.* **2013**, *3*, 1306–1320.

(8) Becker, W.; Weber, Y.; Wetzel, K.; Eirmbtert, K.; Tejedor, F. J.; Joost, H.-G. Sequence characteristics, subcellular localization, and substrate specificity of DYRK-related kinases, a novel family of dual specificity protein kinases. *J. Biol. Chem.* **1998**, *273*, 25893-25902.

(9) Smith, B.; Medda, F.; Gokhale, V.; Dunckley, T.; Hulme, C. Recent Advances in the design, synthesis, and biological evaluation of selective DYRK1A inhibitors: A New avenue for a disease modifying treatment of Alzheimer's? *ACS Chem. Neurosci.* **2012**, *3*, 857–872.

(10) (a) Dirice, E.; Walpita, D.; Vetere, A.; Meier, B.C.; Kahraman, S.; Hu, J.; Dančík, V.; Burns, S.M.; Gilbert, T.J.; Olson, D.E.; Clemons, P.A.; Kulkarni, R.N.; Wagner, B.K. Inhibition of DYRK1A stimulates human β-cell proliferation. *Diabetes* **2016**, 65, 1660-1671. (b) Belgardt, B.F.; Lammert, E. DYRK1A: A promising drug target for islet transplant-based diabetes therapies. *Diabetes* **2016**, *65*, 1496-1498.

(11) (a) Becker, W.; Soppa, U.; Tejedor, F.J. DYRK1A: A potential drug target for multiple Down syndrome neuropathologies. *CNS Neurol. Disord.-Drug Targets* **2014**, *13*, 26–33. (b) Becker, W. Emerging role of DYRK family protein kinases as regulators of protein stability in cell cycle control. *Cell Cycle* **2012**, *11*, 3389–3394.

(12) Ionescu, A.; Dufrasne, F.; Gelbcke, M.; Jabin, I.; Kiss, R.; Lamoral-Theys, D. DYRK1A kinase inhibitors with emphasis on cancer. *Mini Rev. Med. Chem.* **2012**, *12*, 1315-1329.

(13) Abbassi, R.; Johns, T.G.; Kassiou, M.; Munoz, L. DYRK1A in neurodegeneration and cancer: Molecular basis and clinical implications. *Pharmacol. Ther.* **2015**, *151*, 87–98.

(14) Friedman, E. Mirk/DYRK1B in cancer. *J. Cell. Biochem.* **2007**, *102*, 274-279.

(15) Bain, J.; Plater, L.; Elliott, M.; Shpiro, N.; Hastie, C.J.; McLauchlan, H.; Klevernic, I.; Arthur, J.S.; Alessi, D.R.; Cohen, P. The selectivity of protein kinase inhibitors: a further update. *Biochem J.* **2007**, *408*, 297-315.

(16) Göckler, N.; Jofre, G.; Papadopoulos, C.; Soppa, U.; Tejedor, F.J.; Becker, W. Harmine specifically inhibits protein kinase DYRK1A and interferes with neurite formation. *FEBS J.* **2009**, *276*, 6324-6337.

(17) Ogawa, Y.; Nonaka, Y.; Goto, T.; Ohnishi, E.; Hiramatsu, T.; Kii, I.; Yoshida, M.; Ikura, T.; Onogi, H.; Shibuya, H.; Hosoya, T.; Ito, N.; Hagiwara, M. Development of a novel selective inhibitor of the Down syndrome-related kinase Dyrk1A. *Nat. Commun.* **2010**, *1*, 86; DOI: 10.1038/ncomms1090.

(18) Tahtouh, T.; Elkins, J.M.; Filippakopoulos, P.; Soundararajan, M.; Burgy, G.; Durieu, E.; Cochet, C.; Schmid, R.S.; Lo, D.C.; Delhommel, F.; Oberholzer, A.E.; Pearl, L.H.; Carreaux, F.; Bazureau, J.P.; Knapp, S.; Meijer, L. Selectivity, cocrystal structures, and neuroprotective properties of leucettines, a family of protein kinase inhibitors derived from the marine sponge alkaloid leucettamine B. *J. Med. Chem.* **2012**, *55*, 9312-9330.

(19) Anderson, K.; Chen, Y.; Chen, Z.; Dominique, R.; Glenn, K.; He, Y.; Janson, C.; Luk, K.C.; Lukacs, C.; Polonskaia, A.; Qiao, Q.; Railkar, A.; Rossman, P.; Sun, H.; Xiang, Q.; Vilenchik, M.; Wovkulich, P.; Zhang, X. Pyrido[2,3-*d*]pyrimidines: discovery and preliminary SAR of a novel series of DYRK1B and DYRK1A inhibitors. *Bioorg. Med. Chem. Lett.* **2013**, *23*, 6610-6615.

(20) Falke, H.; Chaikuad, A.; Becker, A.; Loaëc, N.; Lozach, O.; Abu Jhaisha, S.; Becker, W.; Jones, P.G.; Preu, L.; Baumann, K.; Knapp, S.; Meijer, L.; Kunick, C. 10-Iodo-11*H*-indolo[3,2-*c*]quinoline-6-carboxylic acids are selective inhibitors of DYRK1A. *J. Med. Chem.* **2015**, *58*, 3131-3143.

(21) Logé, C.; Testard, A.; Thiéry, V.; Lozach, O.; Blairvacq, M.; Robert, J.-M.; Meijer, L.; Besson, T. Novel 9-oxo-thiazolo[5,4-*f*]quinazoline-2-carbonitrile derivatives as dual cyclin-dependent kinase 1 (CDK1)/glycogen synthase kinase-3 (GSK-3) inhibitors: synthesis, biological evaluation and molecular modeling studies. *Eur. J. Med. Chem.* **2008**, *43*, 1469-1477.

(22) Testard, A.; Logé, C.; Léger, B.; Robert, J.-M.; Lozach, O.; Blairvacq, M.; Meijer, L.; Thiéry, V.; Besson, T. Thiazolo[5,4-*f*]quinazolin-9-ones, inhibitors of glycogen synthase kinase-3. *Bioorg. Med. Chem. Lett.* **2006**, *16*, 3419-3423.

(23) Deau, E.; Hédou, D.; Chosson, E.; Levacher, V.; Besson, T. Convenient one-pot synthesis of N^3-substituted pyrido[2,3-*d*]-, pyrido[3,4-*d*]-, pyrido[4,3-*d*]-pyrimidin-4(3*H*)-ones, and quinazolin-4(3*H*)-ones analogs. *Tetrahedron Lett.* **2013**, *54*, 3518-3521.

(24) Leblond, B.; Casagrande, A.-S.; Désiré, L.; Foucourt, A.; Besson, T. DYRK1 inhibitors and uses thereof WO 2013026806. *Chem. Abstr.* **2013**, *158*, 390018.

(25) Foucourt A.; Hédou, D.; Dubouilh-Benard, C.; Girard, A.; Taverne, T.; Désiré, L.; Casagrande, A.-S.; Leblond, B.; Loaëc, N.; Meijer, L.; Besson, T. Design and synthesis of thiazolo[5,4-*f*]quinazolines as DYRK1A inhibitors, Part I. *Molecules* **2014**, *19*, 15546-15571.

(26) Foucourt, A.; Hédou, D.; Dubouilh-Benard, C.; Girard, A.; Taverne, T.; Casagrande, A.-S.; Désiré, L.; Leblond, B.; Besson, T. Design and synthesis of thiazolo[5,4-*f*]quinazolines as DYRK1A inhibitors, Part II. *Molecules* **2014**, *19*, 15411-15439.

(27) Coutadeur, S.; Benyamine, H.; Delalonde, L.; de Oliveira, C.; Leblond, B.; Foucourt, A.; Besson, T.; Casagrande, A.-S.; Taverne, T.; Girard, A.; Pando, M.P.; Désiré, L. A Novel DYRK1A (dual specificity tyrosine phosphorylation-regulated kinase 1A) inhibitor for the treatment of Alzheimer's disease: Effect on tau and amyloid pathologies in vitro. *J. Neurochem*. **2015**, *133*, 440-451.

(28) (a) Abbassi, R.; Johns, T.G.; Kassiou, M.; Munoz, L. DYRK1A in neurodegeneration and cancer: Molecular basis and clinical implications. *Pharmacol. Ther*. **2015**, *151*, 87–98. (b) Casagrande, A.-S.; Bachelot, F.; Throo, E.; Mahé, F.; Leblond, B**.;** Besson, T.; Pando, M. P.; Désiré L. 3D multicellular pancreatic cancer spheroids as drug screening tool for pharmacological evaluation of EHT 5372 and other Mirk/DYRK1B inhibitors. *Cancer Res.* **2014**, *74*, 2620; DOI: 10.1158/1538-7445.AM2014-2620.

(29) Deng, X.; Friedman, E. Mirk kinase inhibition blocks the in vivo growth of pancreatic cancer cells. *Genes Cancer* **2014**, *5*, 337-347.

(30) (a) Deng, X.; Hu, J.; Cunningham, M.J.; Friedman, E. Mirk kinase inhibition targets ovarian cancer ascites. *Genes Cancer* **2014**, *5*, 201–211. (b) Deng, X.; Mercer, S.E.; Sun, C.Y.; Friedman, E. The normal function of the cancer kinase Mirk/dyrk1B is to reduce reactive oxygen species. *Genes Cancer* **2014**, *5*, 22–30. (c) Thompson, B.; Bhansali, R.; Diebold, L.; Cook, D.E.; Stolzenburg, L.; Casagrande, A.-S.; Besson, T.; Leblond, B.; Désiré, L.; Malinge, S.; Crispino, J. D. DYRK1A controls the transition from proliferation to quiescence during lymphoid development by destabilizing Cyclin D3. *J. Exp. Med*. **2015**, *212*, 723-740.

(31) Stotani, S.; Giordanetto, F.; Medda, F. DYRK1A inhibition as potential treatment for Alzheimer's disease. *Future Med. Chem.* **2016**, *8*, 681-693.

(32) Friedman, E. Mirk/Dyrk1B kinase in ovarian cancer. *Int. J. Mol. Sci.* **2013**, *14*, 5560–5575.

(33) Deng, X.; Hu, J.; Ewton, D.Z.; Friedman, E. Mirk/dyrk1B kinase is upregulated following inhibition of mTOR. *Carcinogenesis* **2014**, *35*, 1968–1976.

Table of content graphic